Advances in Geo-Energy Research

Adv. Geo-Energy Res. Vol. 1, No. 3, p. 148-157, 2017
Ausasia Science and Technology Press

Original article

Mechanisms of reservoir pore/throat characteristics evolution during long-term waterflooding

Shoulei Wang[1,2], Xiaodong Han[3,4]*, Yeliang Dong[5], Hongfu Shi[3]

[1]*School of Energy Resources, China University of Geosciences, Beijing 100083, P. R. China*

[2]*Research Institute, China National Offshore Oil Corporation, Beijing 100028, P. R. China*

[3]*Tianjin Branch, China National Offshore Oil Corporation, Tianjin 300459, P. R. China*

[4]*School of Petroleum Engineering, China University of Petroleum (East China), Qingdao 266580, P. R. China*

[5]*No.2 Oil Production Plant of Daqing Oilfield Company Ltd., CNPC, Daqing 163414, P. R. China*

(Received October 11, 2017; revised October 29, 2017; accepted November 3, 2017; published December 25, 2017)

Abstract: Formation pore structure and reservoir parameters change continually during waterflooding due to sand production, clay erosion, and pressure/temperature variation, which causes great challenge in geological modeling and simulation. In this work, the XA Oilfield, a block with more than 20 years' waterflooding history, is used as an example to better understand the fundamental evolution mechanisms of reservoir pore network characteristics over long time waterflooding. We performed a large number of core analyses and experiments to obtain formation parameters (e.g., permeability, porosity, relative permeability, and etc.) at different development stages. The comparison illustrates that reservoir permeability can not only decrease with clay plugging, but also increase by the detachment of fine particles and even the destruction of microscopic structure. We also observed that the point/line contacts among grains decreases, the pore network connectivity increases, the clay content reduces and the rock trends to be more hydrophilic with increasing water injection. Moreover, we developed a pore network model to simulate the variation of formation parameter. The model parameters are also compared and analyzed to get a qualitative understanding of the evolvement laws, which will provide a useful guidance for reservoir accurate modeling.

Keywords: Reservoir parameter variation, permeability, water flooding, pore network model, core analysis.

Citation: Wang, S., Han, X., Dong, Y., et al. Mechanisms of reservoir pore/throat characteristics evolution during long-term waterflooding. *Adv. Geo-Energy Res.* 2017, 1(3): 148-157, doi: 10.26804/ager.2017.03.02.

1. Introduction

Among these improved oil recovery (IOR) techniques, the water flooding is the most popular due to its high efficiency and low expense. During the oilfield development, water is injected into reservoirs to maintain the formation pressure, to sweep oil from the rock surface, and to push it towards production wells (Liu et al., 2012). Although it is commonly believed that the long-term fluid-solid interaction between oil, water and rock, has a tremendous impact on the pore structure (Colón et al., 2004; Crandell et al., 2010), the evolution principles of pore network topology and transport properties are still ambiguous.

Previous literatures mainly concentrate on formation damage caused by the release, migration and deposition of clay particles as well as the inorganic or organic precipitates. This process results in a drastic decrease of permeability and further inhibits oil production (Chang and Civan, 1997). Before exploitation, various types of minerals attach at the pore surface and keep equilibrium in the formation. However, when some chemical substances, such as drilling fluids, brine solution, fracturing liquids, and etc., are injected into formation, the in situ equilibrium condition is disturbed, leading to colloidally induced fines release, migration, and blockage. Even no other fluids is injected, the variations of pressure and temperature also bring about the formation damage through the interaction between various minerals and fluids, such as paraffin and asphaltene deposition (Wang and Civan, 2005). A few phenomenological models have been proposed to describe formation damage caused by water sensitivity, fine particles, and etc (Civan, 1998). Another interesting topic is involved

*Corresponding author. E-mail: hanxiaodongupc@126.com

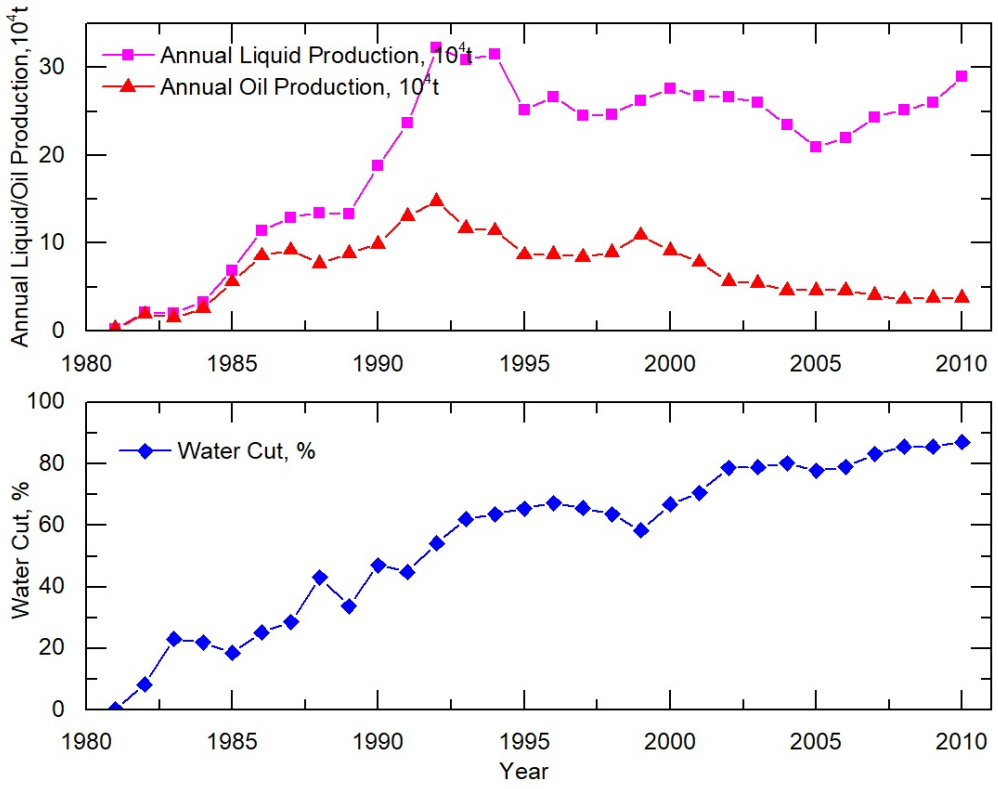

Fig. 1. Production history of the target reservoir.

in the wormhole formation (Fredd and Fogler, 1998, 1999; Szymczak and Ladd, 2009). Mineral dissolution and precipitation reaction in porous media result in pore growth and throat evolution, causing the spontaneous formation of pronounced channels, commonly termed wormholes. They are playing increasingly important roles in engineering, e.g., chemical weathering, diagenesis, and risk assessment of contaminant migration in groundwater (Szymczak and Ladd, 2009). The evolution of wormholes in oil reservoirs are mainly attributed to sand production in loosely consolidated reservoirs or well stimulation like acidification in carbonate formations.

To the best of our knowledge, present studies on the variations of petrophysical properties primarily focused on the characterization of formation damage and optimal condition of wormhole evolution. However, our practical experience from several China oil fields, e.g., Daqing, Shengli, Huabei, and etc., shows a common phenomenon that although wormhole doesn't form in the reservoir, the fluid flow capacity of the formation has improved dramatically in some regions, which is frequently known as thief zone or preferential flow path (Peng et al., 2007; Liu et al., 2010; Wang et al., 2010; Feng et al., 2010, 2011; Wang and Jiang, 2011). For example, in comparison to the perpendicular orientation, injected water tends to flow along the main streamline direction of fluvial facies owing to its good transport capability. Consequently, for a long time, fluid flow interacts with the porous media through a series of comprehensive processes (e.g., detachment, dissolution, migration, and precipitation), resulting in the increment of porosity, permeability in the main streamline direction, and hence thief zone has formed.

In reservoirs with widespread evolution of thief zones, injected water circulates inefficiently and sweeps out of the reservoir rapidly, which will cause unstable displacement with outside oil bypassed. Moreover, thief zone also triggers the premature breakthrough of polymer and some other chemical agents, which prevent the recovery efficiency from being further enhanced. Therefore, thief zone characterization is critical in the development of oil reservoirs, especially those in the high water cut stage. The objective of this work is to study the evolution principles of reservoir pore network characteristics to provide insights into the variation of petrophysical properties during long-term water flooding and shed light on the description of preferential flow path.

2. Background

The target area located in the southern part of XA oilfield is a complex fault block reservoir controlled by geological structure and formation lithology. This reservoir is fan delta deposits, of which the dominant production layers are Dongying Formation and Shahejie Formation. There are many oil-bearing layers on the vertical direction. This reservoir is of serious heterogeneity and the petrophysical properties of each layer are quite different from the others. The initial porosity is 7%∼33% with an average of 21.63% and the initial permeability is $0.04\sim 3680\times10^{-3}$ μm^2 with an average of 310×10^{-3} μm^2. The oil viscosity on the surface is 4∼17 mPa·s.

Table 1. Parameters of these core samples from different development stages.

Time	Porosity (%)	Permeability ($10^{-3}\mu m^2$)	Average Pore Size (μm)	Threshold Pressure (MPa)
1981	8.7∼24.1	1.2∼56.5	0.3∼7	0.133∼1.724
1990	22.1∼26.3	8.4∼1128	2∼13	0.07∼0.31
2004	24.2∼29.2	222∼1280	6∼17	0.06∼0.14

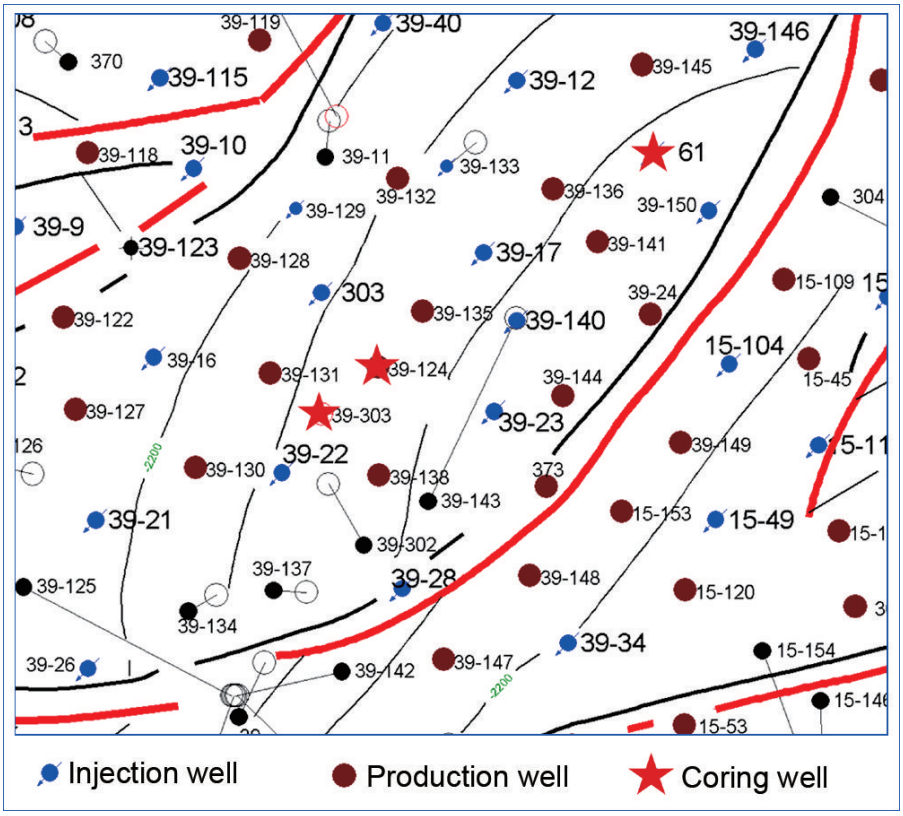

Fig. 2. Locations of coring wells in XA Oilfield.

In Fig. 1, the production history of this block is presented. After twenty years of development, the water cut has reached 87.2%. Production performance and inter-well surveillance reveal that the fluid flow during long-term water flooding has brought tremendous influence on the pore and throat structure, which leads to the variation of the porosity and permeability. To explore the evolvement laws of pore and throat structure, the cores from different development stage are analyzed. These cores from the same segment were obtained from well C61, C39-124, and C39-303 in 1981, 1990 and 2004, respectively. Locations of these coring wells are shown in Fig. 2.

3. Evolution of pore network characteristics

3.1 Pore size distribution

The pore size distribution of these core samples obtained by mercury intrusion method is firstly analyzed. Fig. 3 shows the capillary pressure curves and PSD histograms at different development stages. The corresponding parameters are summarized in Table 1. It is evident that the pore size distribution is experiencing tremendous variation with the development. In 1981, the average pore radius of this layer is only $0.3 \sim 7$ μm, whereas it increases to $2 \sim 13$ μm in 1990 and $6 \sim 17$ μm in 2004, which is more than 3 times as large as the initial value. Moreover, the threshold pressure in 2004 is 10 times less than that in 1981. All these evidences demonstrate that during the long-term water flooding, pore size increases and leads to the improvement of pore network connectivity. This conclusion is in agreement with previous studies (Wang et al., 2013), which reported that with the increase of water cut, pore sizes of all layers increase dramatically in Shengli oil field. When the water cut is 10%, the pore radius of layer 4 is only 9.68 μm; however, when the water cut reaches 90%, the pore radius of this layer increases to 13.02 μm, which is 1.35 times as large as the initial (Fig. 4.). The same conclusion can be obtained from the other layers.

3.2 Porosity and permeability

The variation of pore size distribution eventually leads

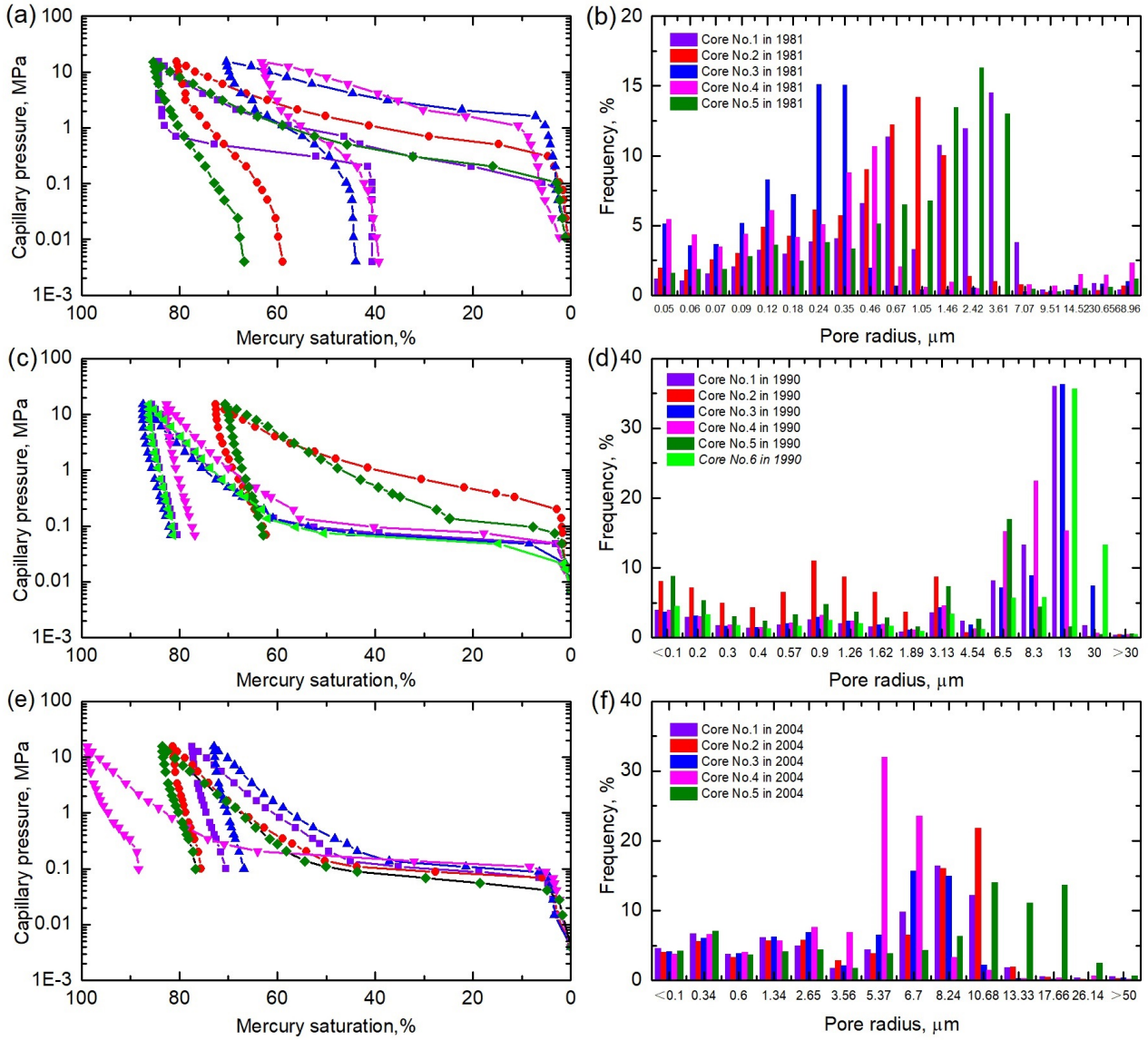

Fig. 3. Capillary pressure curves and pore size distribution histograms from different development stages (a, b) cores obtained from well C61 in 1981; (c, d) cores obtained from well C39-124 in 1990; (e, f) cores obtained from well C39-303 in 2004.

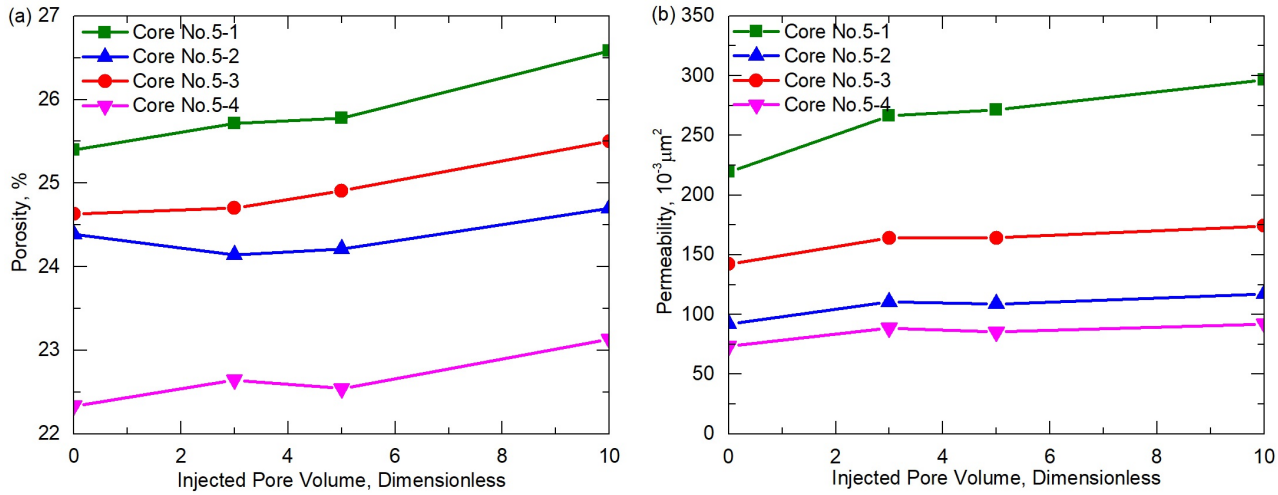

Fig. 4. Variations of porosity (a) and permeability (b) as a function of injected pore volume for cores from C39-124 in water flooding.

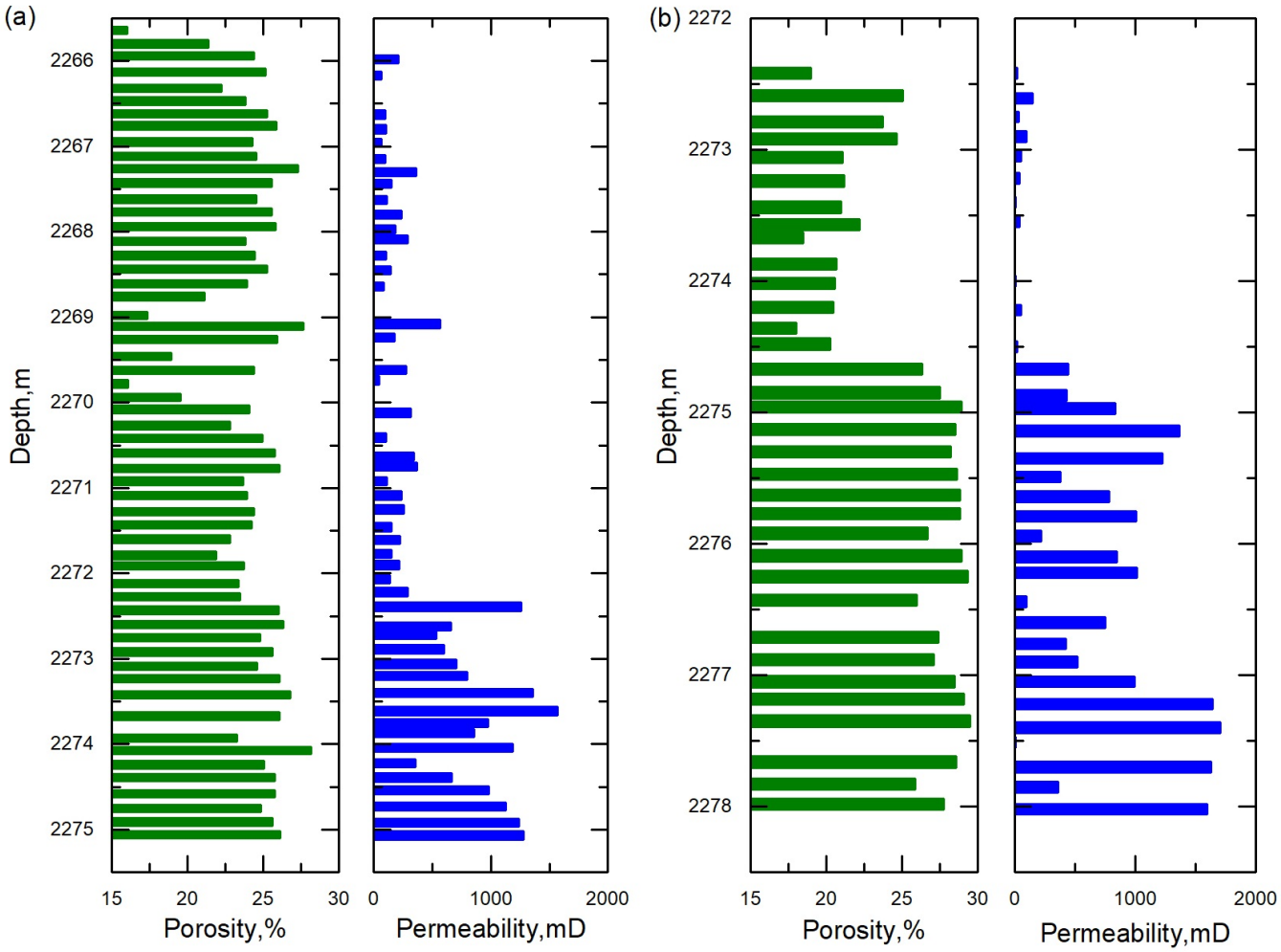

Fig. 5. Porosity and permeability versus depth for well (a) C39-124 and (b) C39-303.

to the variation of the porosity and permeability. Then the variation of permeability and porosity is obtained by the core analysis and experiments. Four core samples from well C39-124 are used to implement the experiments. The porosity and permeability values measured at different pore volumes (PV) of injected water are recorded and presented in Fig. 4.

A general trend is that with the increase of injected pore volume, the porosity of each sample becomes larger. This phenomenon can be attributed to the dissolution and detachment of fine particles which initially attached to the pore surface. Caused by the interaction of injected water, clay particles dissolve or release from the pore surface and flow out of the formation with water. Therefore, the pore space increases and the reservoir porosity becomes larger. Because of the dissolution and detachment of these particles, together with the consequent enlargement of pore size and porosity, the permeability of each sample also increases with water flooding (Fig. 4(b)). This point is verified by the core analysis results shown in Table 1. Moreover, the experiments also demonstrate that the increment degree of the core with higher initial permeability is much larger than that with lower permeability.

Field core analysis is also carried out to study the evolvement laws of permeability in well C39-124 and C39-303. These cores are sampled from the same segment of the two neighbor wells. To some extent, they have similar pore network characteristics. Cores from well C39-124 were acquired during drilling while cores from well C39-303 were obtained after 15 years water flooding. Hence the variation of porosity and permeability can be analyzed by comparing the core analysis results of the two wells at different vertical locations (Fig. 5). This segment is a typical positive rhythm formation, i.e., the permeability is higher at the bottom than that at the top. Fig. 5 indicates that the permeability variations of the top and bottom are different. Permeability at the bottom of this layer, which is of a relatively higher initial value, becomes larger with water flooding, and the permeability increases from $1,200 \times 10^{-3}$ to $1,600 \times 10^{-3}$ μm^2. On the contrary, permeability at the top section with lower initial value decreases with time and the average value changes from 109×10^{-3} to 34×10^{-3} μm^2. This result is consistent with the experimental conclusion. During long-term water flooding, formation with higher initial permeability will increase more than that of the lower ones, due to the dissolution, detachment, and migration of particles. Moreover, the fluid flow capacity for a layer with lower initial permeability, which is of smaller pore size, may even decrease

Table 2. Content variation of clay minerals after water flooding.

Parameter	Injected Pore Volume	Relative Content of Clay Minerals, %				Total Content of Clay Minerals, %
		Kaolinite	Chlorite	Illite	Montmorillonite	
Initial Condition	0	29	34.3	15	21.7	15.7
After Water flooding	15	21.8	27.7	9.2	41.3	11.9

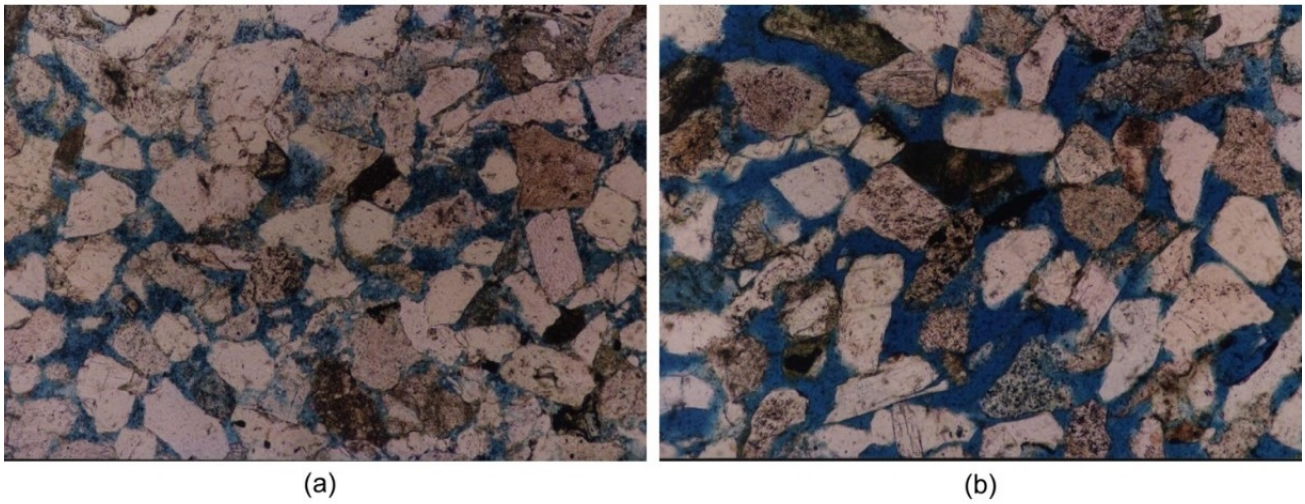

Fig. 6. Thin section image of cores from well C39-124 before (a) and after (b) water flooding. The gray spots represent sand particles while the blue areas correspond to pore space.

for the precipitation of particles and blockage.

3.3 Contact pattern and clay minerals

To gain insight into the microscale resolution of porosity and permeability variation, the evolution of contact pattern among rock particles is analyzed, which has a great impact on the topology and connectivity of pore network. Thin section images of two core samples obtained from well C39-124 at different water cuts are present in Fig. 6. Initially the pore space is very small and the particles make contact with each other mainly in the form of line contact (Fig. 6(a)). However, after long time water flooding, the pore space becomes greater and the proportion of line/point contact decreases. We also noticed that the surface of these particles become cleaner and more particles are surrounded by fluid, which looks like they are floating in the liquid (Fig. 6(b)). The reason can be explained as follows. Because rock consists of clay particles and inorganic or organic precipitates with various sizes and they are connected with each other by the cements, long-term interaction with water leads to the dissolution and erosion of a large proportion of cements and then they are carried out of the formation. Therefore, the microscale connectivity of the formation gets better, which confirms the improvement of formation transport capacity after water flooding. In addition, due to the migration of cements, clay minerals, and some other fine particles, the void space between particles becomes larger and most of the particles keep in the unbound state, thus more pore space is occupied by the injected fluid.

The content variation of clay minerals after water flooding is shown in Table 2. Core analysis manifests that the total content of clay minerals decreases from 15.7% to 11.9% after water flooding. However, the proportions of different clay minerals show distinct variation tendencies. Kaolinite, chlorite, and illite tend to migrate with fluid and consequently, their content in clay minerals decrease with water flooding. Montmorillonite is more likely to have the activity of lattice expansion, and hence its relative content increases from 21.7% to 41.3%.

4. Pore network modeling

For making comparisons with the field data and explaining the inner variation mechanisms of the pore network characteristics, a newly developed pore network modeling method is introduced to simulate the formation parameter variation during water flooding, which takes various particle change into account, such as particle detachment, deposition and movement.

Pore network modeling was firstly proposed by Fatt in 1950s to study microscale multiphase flow behavior. In recent years, there are increasing interests in pore-scale modeling and great progress has been made. Pore network modeling is no longer limited to two-phase flow and the computation of relative permeability curves (Knudsen et al., 2002; Gielen et al., 2004; Joekar-Niasar and Hassanizadeh, 2010, 2011; Jerome and Yannick, 2012; Blunt et al., 2013; Feng et al.,

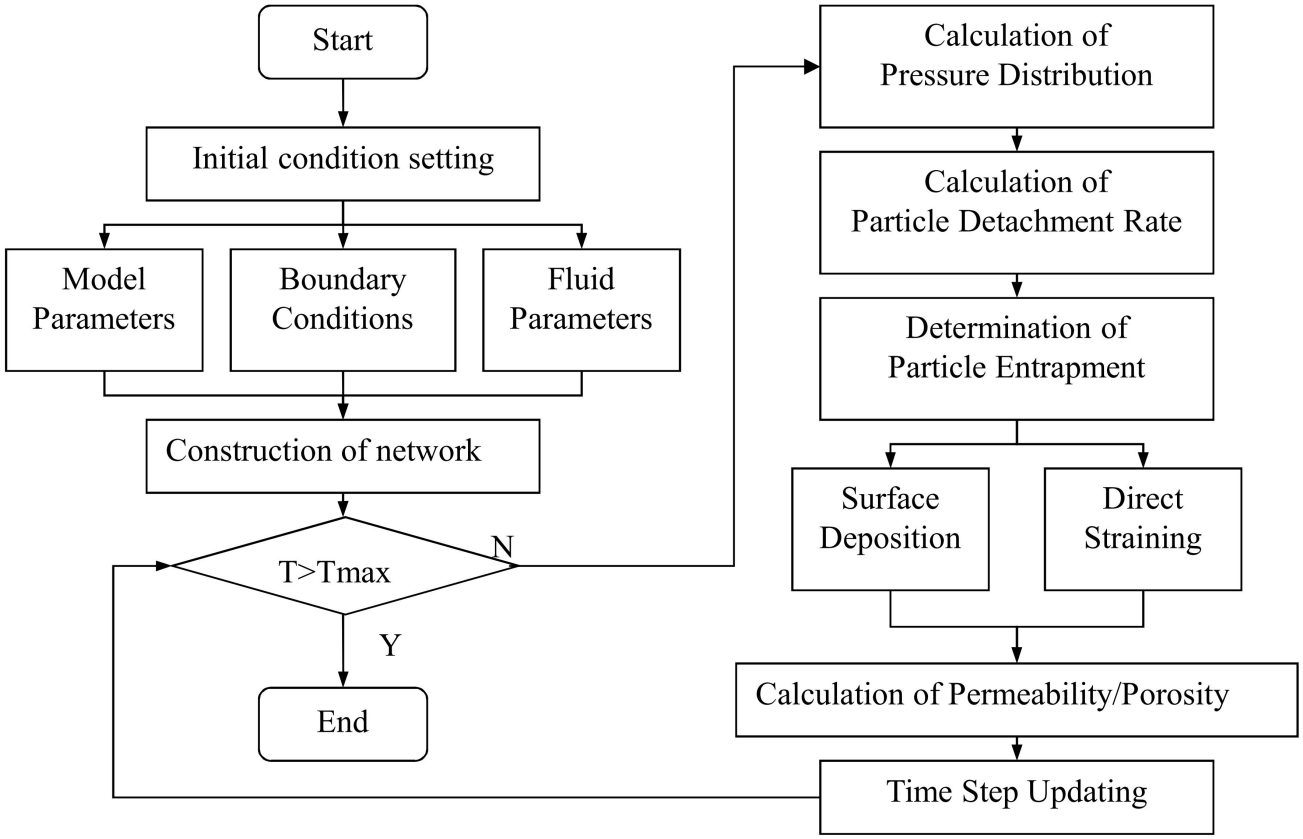

Fig. 7. Computation algorithm of the pore network model.

2015). Effects of wettability, wetting hysteresis, and mass transfer between phases have also been probed by using pore network model. Besides, some more applications have been developed, e.g., modeling of three-phase flow, non-Newtonian fluid, and formation impairment (Feng et al., 2014; Li et al., 2017; Watson et al., 2017). In this section, mechanisms of particles variation and its mathematic description in the proposed pore-network model in introduced in detailed. And some simulation is also conducted for the comparison and validation of the field data.

4.1 Numerical method

4.1.1 Particle detachment

Because injected water exerts drag force on the particles attached on the pore surface, if the velocity gets higher, these particles may detach from the surface and flow out of the reservoir with injected fluid. Then the pore size becomes greater, which will be beneficial for fluid flowing through the reservoir. The mathematical model proposed by Khilar and Fogler (1983) is employed to calculate the detachment rate of particles from the pore surface, r_{ri},

$$r_{ri} = \alpha_i (u_i - u_c) C_{bi} \tag{1}$$

where, r_{ri} is the detachment rate of particles per unit area, $1/(\mathrm{m}^2 \cdot \mathrm{s})$; u_i is the fluid flow rate in the pore, m/s; u_c is the critical fluid flow rate, above which the particles begin to detach, m/s; α_i is the release coefficient and when $u_i \leq u_c$, it equals to zero; C_{bi} is the volumetric concentration of particles on the pore/throat surface, dimensionless.

4.1.2 Particle deposition

Particles flowing with injected water may also precipitate and attach on the pore surface again or remain at the pore/throat entrance which will result in blockage. The main entrapment mechanisms include surface deposition, direct blockage, and bridging. Surface deposition means that detached particles with smaller size may reattach to the pore/throat surface under the action of gravity and/or electric forces, causing the decrease of pore/throat radius. We use the following equation to characterize particle deposition in the pore network (Jalel and Jean-Francois, 1999):

$$r_{ci} = 6\pi r_i^2 u_i \left(\frac{d_p}{L_i}\right) C_{fi} \tag{2}$$

where, r_{ci} is the deposition rate of particles per unit pore surface area, $1/(\mathrm{m}^2 \cdot \mathrm{s})$; r_i is the radius of pore/throat, m; d_p is the particle radius, m; L_i is the throat length, m; C_{fi} is the volumetric particle concentration of the fluid in pore space, dimensionless. When particles flow through a pore or

throat whose radius is smaller than theirs, the particle will be entrapped at the entrance and make the pore/throat blocked. This process is termed direct blockage. Particle bridging means that several particles whose radii smaller than that of their passing throat could plug the throat by bridging at its entrance. Generally, if the particle size is larger than 1/3 of its passing throat, bridging takes place and results in the blockage.

4.1.3 Particle movement

According to the experimental results conducted by Rege and Fogler (1987), the moving velocity difference between particles and the fluids in the pore-throat could be neglected which indicates we can take these two velocity as equal. So, the particles are assumed to be distributed evenly and have the same moving velocity as the fluid that it flows in.

Computation algorithm for our pore network model is shown in Fig. 7. Details of the simulation can be found in Feng's work (2013). Based on the pore network modeling, a series of simulation is carried out for analyzing the pore size distribution and porosity and permeability change after waterflooding. Detailed results are shown as follows.

4.2 Pore size distribution

Fig. 8 and Table 3 show the pore-throat radius variation value before and after waterflooding. We can see from the simulation results that the pore-throat distribution has minor change after waterflooding and the radius has the trend of increase. And the results are consisted with the field data shown in Section 3.1. The pore-throat radius variation trend could be explained by considering different kinds of particle variation mechanisms. In the process of waterflooding, the clay particles attached on the pore-throat surface would be detached with the influence of drag force, which will result in the increase of the pore-throat radius. Meanwhile, the detached particles may deposit in part of the pore-throat surface and result in the consequent decrease of relevant pore-throat radius. That is why the pore-throat radius distribution would have minor change after waterflooding for a long time.

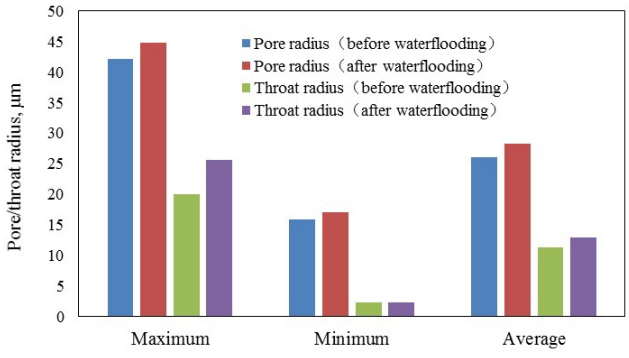

Fig. 8 . Comparison of simulated pore-throat radius value before and after waterflooding.

4.3 Porosity and permeability

Based on the simulation results about pore-throat radius variation, the porosity and permeability variation after waterflooding is also studied here for making comparison with the analyzed field data. In this part, we perform simulations to study formation variations under different pressure gradients. As shown in Fig. 9(a), for a constant pressure gradient, the network permeability increases gradually and the variation curve asymptotically converges to a constant value after long-term waterflooding. For simulations at different pressure gradients, the permeability increase more quickly at higher pressure gradient. Fig. 9(b) reveals that the variation principle of porosity is similar to that of permeability. Our simulation results are consistent with the conclusions obtained from core analyses and waterflooding experiments. The results are also consistent with the field data in Section 3.2.

5. Conclusions

Core analyses and displacement experiments of XA oil field show that during long-term water flooding, caused by the dissolution and detachment of fine particles and clay minerals, the pore/throat size becomes larger and the proportion of line/point contact decreases, which lead to the improvement of pore network connectivity and the enlargement of porosity and permeability. The transport capacity of the formation with higher initial permeability will increase more than that of the lower. But the fluid flow capacity of porous media with lower original permeability may even decrease for the precipitation of particles and blockage.

Moreover, after long-time interaction with injected water, the total content of clay minerals decreases dramatically. The relative contents of kaolinite, chlorite, and illite reduce while the proportion of montmorillonite increases. The variation of pore network topology also brings about the change of multi-phase flow capability. Consequently, the hydrophilicity of the rock is enhanced and the relative permeability curves move rightward.

A pore network model, which takes into account the detachment and entrapment of fine particles, is employed to predict the formation parameters variation. Our simulation results are in accordance with the conclusions obtained from core analyses and experiments.

Nomenclature

r_{ri} = the detachment rate of particles per unit area, $1/(\mathrm{m}^2/\mathrm{s})$

u_i = the fluid flow rate in the pore, m/s

u_c = the critical fluid flow rate, m/s

C_{bi} = the volumetric concentration of particles on the pore/throat surface, dimensionless

r_{ci} = the deposition rate of particles per unit pore surface area, $1/(\mathrm{m}^2/\mathrm{s})$

r_i = the radius of pore/throat, m

d_p = the particle radius, m

L_i = the throat length, m

Table 3. Variation of pore-throat radius before and after water displacement.

Parameter	Before waterflooding		After waterflooding	
	Pore radius (μm)	Throat radius (μm)	Pore radius (μm)	Throat radius (μm)
Maximum	42.18	19.95	44.74	25.65
Minimum	15.91	2.33	17.09	2.31
Average	26.07	11.39	28.23	12.88

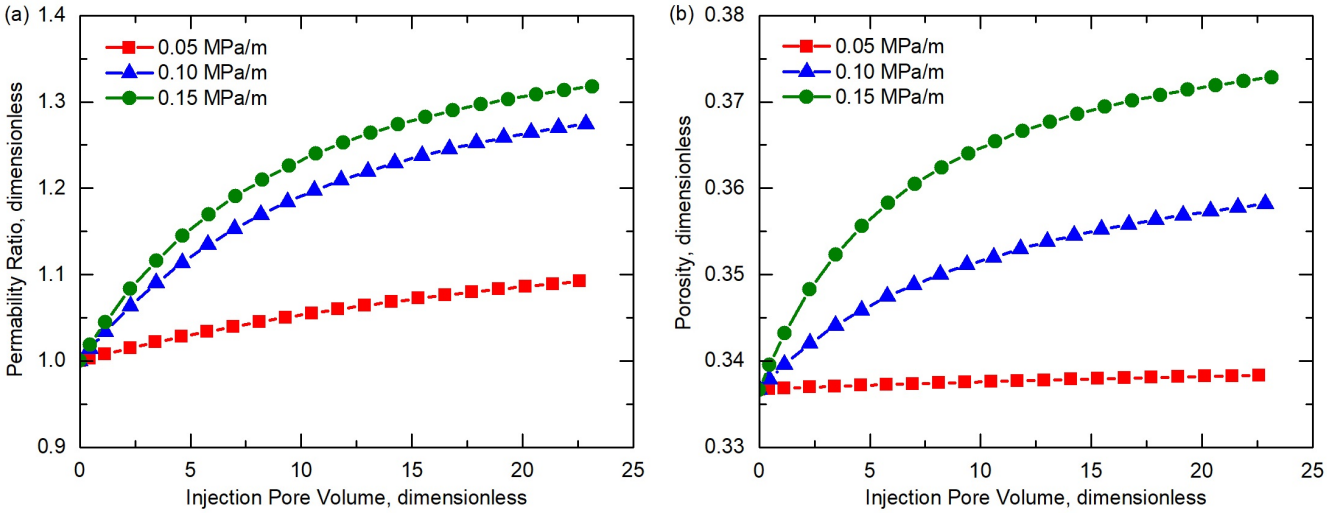

Fig. 9 . Variation of permeability (a) and porosity (b) under various pressure gradients obtained by using pore network model.

C_{fi} = the volumetric concentration of the fluid in pore space, dimensionless

Acknowledgments

This research was conducted under the support of the National Science and Technology Major Project of China (Grant No. 2016ZX05016).

References

Blunt, M.J., Bijeljic, B., Dong, H., et al. Pore-scale imaging and modelling. Adv. Water Resour. 2013, 51: 197-216.

Chang, F.F., Civan, F. Practical model for chemically Induced formation damage. J. Pet. Sci. Eng. 1997, 17(1-2): 123-137.

Civan, F. Incompressive cake filtration: Mechanism, parameters, and modeling. AIChE J. 1998, 44(11): 2379-2387.

Civan, F. Formation damage mechanisms and their phenomenological modeling–An overview. Paper SPE 107857 Presented at European Formation Damage Conference, Scheveningen, The Netherlands, 30 May-1 June, 2007.

Colón, C.F.J., Oelkers, E.H., Schott, J. Experimental investigation of the effect of dissolution on sandstone permeability, porosity, and reactive surface area. Geochim. Cosmochim. Acta 2004, 68(4): 805-817.

Crandell, L.E., Peters, C.A., Um, W., et al. Changes in the pore network structure of Hanford sediment after reaction with caustic tank wastes. J. Contam. Hydrol. 2010, 131(14): 89-99.

Ding, S., Jiang, H., Liu, G., et al. Determining the levels and parameters of thief zone based on automatic history matching and fuzzy method. J. Pet. Sci. Eng. 2016, 138: 138-152.

Feng, Q., Han, X., Wang, S., et al. 3D network simulation study of the formation parameter variation sand reservoir during waterflooding process. Petroleum Geology and Recovery Efficiency 2013, 20(4): 79-82. (in Chinese)

Feng, Q., Han, X., Wang, S., et al. Network simulation of formation damage due to suspended particles in injection water. Journal of Southwest Petroleum University (Science & Technology Edition) 2014, 36(3): 179-184. (in Chinese)

Feng, Q., Li, S., Han, X.D., et al. Network simulation for formation impairment due to suspended particles in injected water. J. Pet. Sci. Eng. 2015, 133: 384-391.

Feng, Q., Wang, S., Gao, G., et al. A new approach to thief zone identification based on interference test. J. Pet. Sci. Eng. 2010, 75 (1-2): 13-18.

Feng, Q., Wang, S., Wang, S., et al. Identification of thief zones by dimensionless pressure index in waterfloods. Paper SPE 143926 Presented at SPE Enhanced Oil Recovery Conference, Kuala Lumpur, Malaysia, 19-21 July, 2011.

Fredd, C.N., Fogler, H.S. Influence of transport and reaction on wormhole formation in porous media. AIChE J. 1998, 44(9): 1933-1949.

Fredd, C.N., Fogler, H.S. Optimum conditions for wormhole formation in carbonate porous media: Influence of transport and reaction. SPE J. 1999, 4(3): 196-205.

Gielen, T., Hassanizadeh, S.M., Celia, M.A., et al. A pore-scale network approach to investigate dynamic effects in multiphase flow. Dev. Water Sci. 2004, 55: 83-94.

Jalel, O., Jean-Francois, V. A two-dimensional network model to simulate permeability decrease under hydrodynamic effect of particle release and capture. Transp. Porous Media 1999, 37(3): 303-325.

Joekar-Niasar, V., Hassanizadeh, S.M. Effect of fluids properties on non-equilibrium capillarity effects: Dynamic pore-network modeling. Int. J. Multiph. Flow 2011, 37(2): 198-214.

Joekar-Niasar, V., Hassanizadeh, S.M., Dahle, H.K. Non-equilibrium effects in capillarity and inter facial area in two-phase flow: Dynamic pore-network modeling. J. Fluid Mech. 2010, 655(1): 38-71.

Khilar, K.C., Fogler, H.S. Water sensitivity of sandstones. SPE J. 1983, 23(1): 55-64.

Knudsen, H.A., Aker, E., Hansen, A. Bulk flow regimes and fractional flow in 2d porous media by numerical simulations. Transp. Porous Media 2002, 47(1): 99-121.

Li, D., Yang, J., Lu, D. Thief zone identification based on transient pressure analysis: A field case study. J. Pet. Explor. Dev. 2016, 6(1): 63-72.

Li, J., McDougall, S.R., Sorbie, K.S. Dynamic pore-scale network model (PNM) of water imbibition in porous media. Adv. Water Resour. 2017, 107: 191-211.

Liu, H., Li, G., Li, Y. Simulation of formation damage after long term water flooding. Paper SPE 158409 Presented at SPE Asia Pacific Oil and Gas Conference and Exhibition, Perth, Australia, 22-24 October, 2012.

Liu, Y., Bai, B., Wang, Y. Applied technologies and prospects of conformance control treatments in China. Oil Gas Sci. Technol. 2010, 65(6): 859-878.

Lux, J., Anguy, Y. A study of the behavior of implicit pressure explicit saturation (IMPES) schedules for two-phase flow in dynamic pore network models. Transp. Porous Media 2012, 93(1): 203-221.

Peng, S., Shi, Y., Han, T., et al. A quantitative description method for channeling path of reservoirs during high water cut period. Acta Petrolei Sinica 2007, 28(5): 79-84. (in Chinese)

Rege, S.D., Fogler, H.S. Network model for straining dominated particle entrapment in porous media. Chem. Eng. Sci. 1987, 42(7): 1553-1564.

Shokri, A.R., Babadagli, T. Field scale modeling of CHOPS and solvent/thermal based post CHOPS EOR applications considering non-equilibrium foamy oil behavior and realistic representation of wormholes. J. Pet. Sci. Eng. 2016, 137: 144-156.

Szymczak, P., Ladd, A.J.C. Wormhole formation in dissolving fractures. J. Geophys. Res. 2009, 114(B6): B06203.

Wang, H., Jiang, M., Zhang, J., et al. Simulation on variation of physical properties in high water cut reservoir. Acta Petrolei Sinica 2004, 25(6): 53-58. (in Chinese)

Wang, S., Feng, Q., Han, X. A hybrid analytical/numerical model for the characterization of preferential flow path with non-Darcy flow. PLOS ONE 2013, 8(12): e83536.

Wang, S.J., Civan, F. Modeling formation damage by asphaltene deposition during primary oil recovery. J. Energy Resour. Technol. 2005, 127(4): 310-317.

Wang, S.L., Jiang, H.Q. Determine level of thief zone using fuzzy ISODATA clustering method. Transp. Porous Media 2011, 86(2): 513-520.

Wang, X.Z., Wang, J.Y., Wang, C.F., et al. Quantitative description of characteristics of high-capacity channels in unconsolidated sandstone reservoirs using in situ production data. Pet. Sci. 2010, 7(1): 106-111.

Watson, M.G., Bondino, I., Hamon, G., et al. A pore-scale investigation of low-salinity waterflooding in porous media: Uniformly wetted systems. Transp. Porous Media 2017, 118(2): 201-223.